Enhanced quantum sensitivity in a vibrating diatomic molecule due to a rotational amendment

Suranjana Ghosh* and Utpal Roy†
Indian Institute of Technology Patna, Patliputra Colony, Patna 800013, India
(Received 18 August 2013; revised manuscript received 17 May 2014; published 18 August 2014)

Quantum sensitivity is an important issue in the field of quantum metrology where sub-Planck scale structures play a crucial role in the Heisenberg limited measurement. We investigate the mesoscopic superposition structures, particularly for well-known catlike and compasslike states, in the rotating Morse system where sub-Planck scale structures originate in the dynamics of a suitably constructed SU(2) coherent state. A detail study of the sensitivity analysis reveals that rotational coupling in the vibrational wave packet can be used as a probe to enhance the sensitivity limit in a diatomic molecule. The maximum sensitivity limit is identified with the rotational amendment, and a quantitative measure of the angle of rotation for different rotational levels is also given. The correspondence of the numerical result with the angle of rotation is also delineated in phase-space Wigner representation.

DOI: 10.1103/PhysRevA.90.022113 PACS number(s): 03.65.−w, 42.50.Md, 42.50.Dv

I. INTRODUCTION

Improvement in parameter estimation has often led to scientific breakthroughs and technological advancement. Recent advances in experimental techniques allow us access to unprecedented levels of control over quantum systems. Quantum metrology is the field which exactly deals with the fundamental limits to measurement [1]. To reach the ultimate sensitivity limit, one can repeat the measurement process N times and take the average over the outcomes. It reduces the error which scales as $1/\sqrt{N}$, known as the standard quantum limit. This is the ultimate limit one can reach using classical properties. To push this boundary, one needs the help of quantum properties. In quantum metrology, special states, such as entangled or squeezed states, have been employed for estimation of these parameters to beat the standard quantum limit [1,2]. In this case, the sensitivity can be enhanced $\sqrt{N}$ times and can reach the Heisenberg limit. On the other hand, the Planck scale executes a fundamental role in quantum mechanics. Phase-space quasiprobability distributions of certain quantum superposition states reveal structures on a scale that is smaller than the Planck dimension. The existence and importance of these small structures (called sub-Planck structures) were first pointed out in Ref. [3]. These smallest interference (sub-Planck scale) structures play a crucial role in high-precision parameter estimation and Heisenberg limited measurement. Recently, sub-Planck scale structures have drawn considerable attention and have been found in different situations [4–14]. In all of these studies, the sub-Planck interference phenomena appear with a suitable combination of appropriate superposition of coherent states (CSs) [15]. In our earlier studies, we found the existence of sub-Planck structures in a molecular system and showed their decoherence sensitivity [7,10]. It involved the vibrational motion of a diatomic molecule described by the evolution of a suitable wave packet. Governed by a nonlinear energy spectrum, the initial wave packet breaks into mesoscopic superpositions at a later time and gives rise to sub-Planck structures in phase space.

In recent years, vibrational dynamics of diatomic molecules has gained importance due to its potential application in quantum computation. For example, ultrafast Fourier transforms can be performed using a femtosecond laser-driven molecule [16,17]. High-precision molecular wave-packet interferometry has been used to read and write the amplitude and phase information of wave functions [18,19], which is a vital task for quantum information processing and the development of quantum gates.

A key concern, however, is the effect of rotational coupling on the vibrational motion of diatomic molecules. Our goal is to study the sensitivity limit vis-á-vis sub-Planck structures in phase space by introducing the rotational coupling with the vibrational motion of a diatomic molecule. Visualization of the rovibrational dynamics needs a three-dimensional scenario [20–22], hence it is difficult to observe its dynamics in phase space which will require a six-dimensional configuration. To unravel this intricacy, we recall an appropriate model, called the rotating Morse system, which can describe the rotational and vibrational coupling nicely in one-dimensional symmetry [23–25]. The energy eigenstates of a rotating Morse system in phase space are elucidated in Ref. [26]. To the authors' knowledge, there is no study about the wave-packet dynamics of this system in phase space. In this study, we choose a model [25] where the effective potential becomes minimum around a certain equilibrium internuclear distance, which is a function of the rotational quantum number j. This can satisfactorily describe the coupling between the two degrees of freedom, i.e., the rovibrational interplay. This coupling is also captured in mesoscopic superpositions states, such as catlike states and compasslike states [27,28]. The most sensitive structures in phase space, called sub-Planck scale structures, are found to determine the sensitivity limit of a quantum state. We have chosen the example of an iodine molecule (I_2), which is a uniquely suited seed molecule for laser-induced fluorescence, and an appropriate CS wave packet is constructed to see the system dynamics. We show the amendment in vibrational wave-packet dynamics due to the presence of rotational coupling. Significant advances have been made in manipulating and controlling rotational population in rovibrational wave packets by using shaped femtosecond pulses [29] and wave-packet interference [30]. To make the effect of rotational coupling transparent, we

*sghosh@iitp.ac.in
†uroy@iitp.ac.in

have considered a single rotational level for a rovibrational wave packet [22]. The sub-Planck dimension in mesoscopic superposition structures is found to vary with the rotational quantum number j. Maximum sensitivity is achieved for a particular value of j and a scheme is provided to find the exact orientation of the corresponding system in phase space. Additionally, the corresponding phase-space Wigner distribution is numerically calculated and delineated in phase space to further verify the orientation and the structures in the maximum sensitive state.

The paper is organized as follows. We present a brief overview of a 1D rotating Morse system and its validity. We construct the corresponding SU(2) CS wave packet to analyze the dynamics of the CS and to explain the effect of rovibrational coupling in configuration space. In Sec. III, we study the rotational sensitivity in a vibrating diatomic molecule through mesoscopic superposition structures. Specifically, we have focused on catlike and compasslike states where the sensitivity issue is explored at the sub-Planck level. The scaling law is verified and the maximum sensitivity limit is achieved for rotational amendment. A quantitative measure of the angle of rotation in phase space is also depicted. Furthermore, a numerical study shows the phase Wigner distribution, which reveals a nice correspondence with the angle of rotation. Finally, we end up with some conclusions in Sec. IV.

II. DYNAMICS OF COHERENT STATE IN ROTATING MORSE POTENTIAL

We start with the effective potential $V_{\mathrm{eff}}(r)$, known as the rotating Morse potential,

$$V_{\mathrm{eff}}(r) = D[e^{-2\beta(r-r_0)} - 2e^{-\beta(r-r_0)}] + \frac{j(j+1)\hbar^2}{2\mu r^2}. \quad (1)$$

The first part describes the well-known Morse potential, an appropriate model for a vibrating diatomic molecule. D is the dissociation energy of the molecule, r_0 is the equilibrium internuclear separation, and β is the range parameter. The second part stands for the centrifugal contribution of rotation. A description of the system can be obtained with a modified equilibrium internuclear distance r_j and a dissociation energy D_j [25]. Using a semianalytical method [23], one can find

$$r_j = r_0\left(1 + \frac{A}{\beta^2 r_0^2 D}\right), \quad D_j = D - A\left(1 - \frac{A}{\beta^2 r_0^2 D}\right), \quad (2)$$

where $A = \frac{j(j+1)\hbar^2}{2\mu r_0^2}$. We define $A_j = \frac{j(j+1)\hbar^2}{2\mu r_j^2}$ and expand the centrifugal term of Eq. (1) around $r = r_j$. Keeping terms up to second order, the Schrödinger equation is solved to obtain the eigenfunctions of the rotating Morse system as

$$\psi_{n,j}(y) = N_{n,j} e^{-y/2} y^b L_n^{2b}(y), \quad (3)$$

where the variable y: $y = 2\lambda_j e^{-\beta(r-r_0)} = 2\lambda_j u e^{-\beta(r-r_j)}$ ($0 < y < \infty$) and $u = e^{-\beta(r_j - r_0)}$. n is the vibrational quantum number, $L_n^{2b}(y)$ stands for the associated Laguerre polynomial, $b = \sqrt{(c_0 - E_{v,j})\lambda_j^2/c_2}$, and $\lambda_j = \sqrt{\frac{2\mu c_2}{\beta^2\hbar^2}}$. Here the constants are expressed as $c_0 = 3A_j b_j^2 - 3A_j b_j + A_j$, $c_1 = (3A_j b_j^2 - 2A_j b_j + uD)/u$, $c_2 = (3A_j b_j^2 - A_j b_j + u^2 D)/u^2$, and $b_j = (\beta r_j)^{-1}$ are dependent on quantum number j. Defining $\bar{\lambda}_j = \frac{c_1}{c_2}\lambda_j$, one obtains the constraint condition, $2b + 2n = 2\bar{\lambda}_j - 1$. $N_{n,j}$ is the normalization constant: $N_{n,j} = [\frac{\beta(2\bar{\lambda}_j - 2n - 1)\Gamma(n+1)}{\Gamma(2\bar{\lambda}_j - n)}]^{1/2}$.

The rovibrational energy eigenvalues $E_{n,j}$ turn out as

$$E_{n,j} = 2\frac{c_1}{\lambda_j}(n + 1/2) - \frac{c_2}{\lambda_j^2}(n + 1/2)^2 + c_0 - \frac{c_1^2}{c_2}. \quad (4)$$

It is worth pointing out that in the absence of rotation, $c_0 = 0$, $c_1 = c_2 = D$, the system describes a vibrating diatomic molecule, i.e., the well-known Morse potential.

Alternatively, one can compute r_j numerically by solving the transcendental equation

$$\left.\frac{dV_{\mathrm{eff}}(r)}{dr}\right|_{r=r_j} = 0. \quad (5)$$

These two sets of r_j's are plotted in Fig. 1(a), which show very good agrement for $j < 160$ for the I_2 molecule. It shows that the rotational motion increases the equilibrium distance [Fig. 1(a)] and decreases the dissociation energy [Fig. 1(b)]. Physically, in the presence of the rotational centrifugal force, the two constituent atoms of a diatomic molecule tend to settle at a larger distance and are more prone to dissociate, reducing the amount of energy required to make them independent.

We construct a rovibrational wave packet of the I_2 molecule, which is a CS, dependent on the particular rotational quantum number. Many theoretical and experimental investigations have been carried out on this molecule, in particular, Zewail and co-workers investigated rovibrational wave-packet dynamics in the well-characterized electronic $B0_u^+$ state [31]. Lohmüller *et al.* [22] discussed the pump-probe experiment of I_2 at room temperature and the detection of fractional revivals using a full-dimensional quantum wave packet. Here, we consider an initial rovibrational wave packet which is centered around the 10th vibrational energy level with $j = 45$. Under the laser polarizations magic angle conditions [22], it takes into account the vibrational as well as the rotational motions. Once the bound states of the potential are included, the dynamical symmetry group becomes SU(2). For Morse system, the corresponding SU(2) generators are given [32]. In this case, we find

$$\hat{J}_+ = \left[\frac{d}{dy}(2b-1) + \frac{1}{y}b(2b-1) - \bar{\lambda}_j\right]\sqrt{\frac{b-1}{b}},$$
$$\hat{J}_- = -\left[\frac{d}{dy}(2b+1) - \frac{1}{y}b(2b+1) + \bar{\lambda}_j\right]\sqrt{\frac{b+1}{b}}, \quad (6)$$
$$\hat{J}_0 = \left[y\frac{d^2}{dy^2} + \frac{d}{dy} - \frac{b^2}{y} - \frac{y}{4} + n + 1/2\right].$$

$\hat{J}_0$ is the projection operator of the angular momentum m: $m = n - \bar{\lambda}_j + 1/2$. We obtain the SU(2) CS by operating the displacement operator $\exp(\alpha\hat{J}_+ - \alpha^*\hat{J}_-)$ on the highest bound state n', defined by $\hat{J}_+\psi_{n',j}(y) = 0$, where α is the CS parameter. Temporal evolution of the CS wave packet is given, in the eigenfunction basis, by

$$\Phi(y,t) = \sum_{n=0}^{n'} d_n^j\, \psi_{n,j}(y) e^{-iE_{n,j}t}, \quad (7)$$

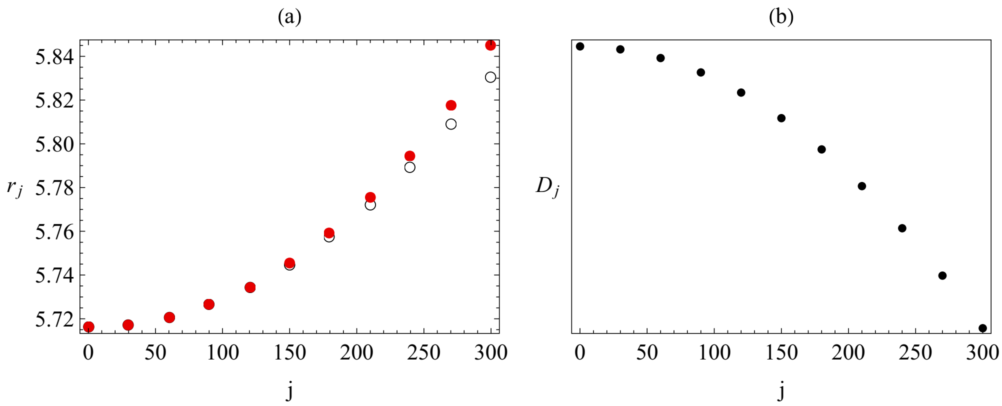

FIG. 1. (Color online) (a) The variation of r_j with the rotational quantum number j. It implies that the numerical values, obtained by solving the transcendental Eq. (5) (red filled circles) match nicely with the approximate values from Eq. (2) (black circles). It starts to differ for higher values of j (>160). (b) The change of the dissociation energy of the effective potential with j. We have chosen the I_2 molecule where $\beta = 0.9605$ a.u.$^{-1}$, reduced mass $\mu = 11.56 \times 10^4$ a.u., $r_0 = 5.716$ a.u., and $D = 0.0198$ a.u.

where the weighting coefficients are evaluated as

$$d_n^j = \frac{(-\alpha)^{n'-n}}{(n'-n)!}\left[\frac{n'!\Gamma(2\bar{\lambda}_j - n)}{n!\Gamma(2\bar{\lambda}_j - n')}\right]^{\frac{1}{2}}. \tag{8}$$

The presence of a nonlinear term in the energy expression leads to interesting phenomena, called fractional revivals, which occur at some specific instances between two full revivals [33,34]. The short-time evolution displays a classical periodicity. The classical and revival time periods are, respectively, given by

$$T_{cl} = \frac{2\pi\lambda_j}{2c_1 - c_2/\lambda_j} \text{ and } T_{\rm rev} = 2\pi\lambda_j^2/c_2. \tag{9}$$

At fractional revival times $(\bar{p}/\bar{q})T_{\rm rev}$ (where $\bar{p}$ and $\bar{q}$ are mutually prime integers), the wave packet breaks into a number of subsidiary wave packets. For even (odd) values of $\bar{q}$, the wave packet breaks into $\bar{q}/2$ ($\bar{q}$) parts. In the inset of Fig. 2, the 10th vibrational energy levels for different rotational numbers are zoomed and the rovibrational coupling effect is shown at $t = 0.25\ T_{\rm rev}$, when CS is split into two parts. For $j = 0$, the two parts are situated at 5.3 and 6.48 a.u. (dark filled plot). For $j = 45$, they come close to each other, situated at 5.62 and 6.36 a.u., respectively (dashed line). For a greater value of j ($j = 65$), the position-space probability structure looks completely different and shows oscillatory structure (light filled plot). The interpretation lies in the fact that the two split CSs oscillate inside the potential well in a back-and-forth motion. In the first quarter of the oscillation, they approach each other, while in the next quarter, they recede. At the halfway point of the oscillation, they are reflected from the potential well with a phase change of π and again become counterpropagating. For $j = 65$, they overlap each other in the course of their oscillation and produce the oscillatory ripples, clearly visible in the inset of Fig. 2. A single interference ripple has dimension ~0.1 a.u. or 5.3 picometers. Although the experimental observation of small quantum interference structures is very challenging, similar interference ripples in the picometer scale were recently visualized experimentally for the I_2 molecule [35,36].

III. ROTATIONAL SENSITIVITY

Until now, we have explored the wave-packet dynamics in position space only. For a better description, we present a phase-space picture of the dynamics. Here, we make use of the Wigner function [37], which is defined as

$$W(r,p,t) = \frac{1}{\pi\hbar}\int_{-\infty}^{+\infty} \Phi'^{*}(r-r',t) \times \Phi'(r+r',t)e^{-2ipr'/\hbar}dr'. \tag{10}$$

Here, $\Phi'(r,t)$ is the coherent state as a function of r. This Wigner function presentation can reveal interesting mesoscopic superposition structures of the CS at different times.

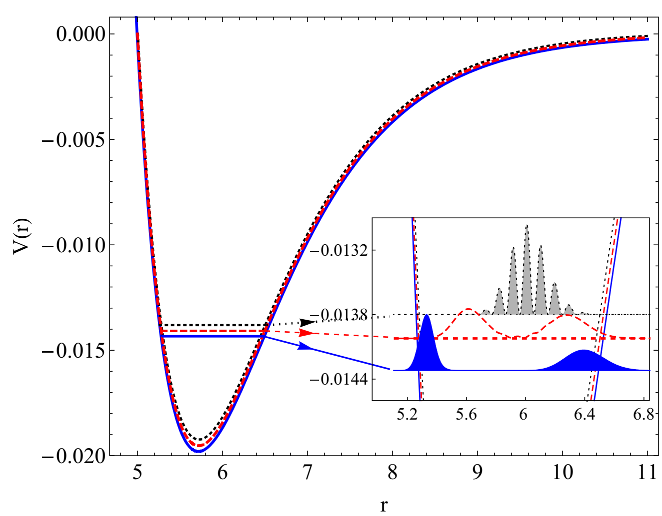

FIG. 2. (Color online) Effective potentials for $j = 0$ (solid line), $j = 45$ (dashed line), and $j = 65$ (dotted line) are depicted. Inset: Zoom of the corresponding 10th energy levels, where the wave packets at $t = 0.25\ T_{\rm rev}$ are shown as dark filled ($j = 0$), dashed ($j = 45$), and light filled ($j = 65$) plots, respectively. The potential and the internuclear distance are in atomic units. The corresponding parameter values are $\beta = 0.9605$ a.u., reduced mass $\mu = 11.56 \times 10^4$ a.u., $r_0 = 5.716$ a.u., $D = 0.0198$ a.u., and $\alpha = 1.6$.

In addition to its positive regions, the Wigner function can also possess negative regions for nonclassical states. In the course of time evolution, one obtains the Schrödinger catlike state at 1/4th of the revival time. Four-way breakup or the compasslike state emerges at 1/8th of the revival time. Sub-Planck scale structures appear in the Wigner function at the interference region of these mesoscopic superposition states. These structures are alternate tiles of maxima and minima. For symmetric potentials such as the harmonic oscillator, these tiles are rectangular in shape and one can easily find the area of these structures by multiplying two side arms, by measuring the distances between the zeros of the Wigner function. However, for an asymmetric potential, it is quite nontrivial. We find the zeros of the Wigner function around a particular structure (either positive or negative) by projective plots of the Wigner function in both the conjugate coordinates. Then we perform a set of measurements and, finally, take the average. The smallest sub-Planck structures are formed due to the superposition of off-diagonal superposition structures in a compasslike state.

In addition to the above procedure, one can follow an alternative methodology, mentioned in one of our papers [11]. The idea is as follows: In typical experimental situations, a small perturbation can be applied through a weak constant force, which will physically shift the state in phase space. This can be mathematically incorporated by finding an appropriate displacement operator for the coherent state, then applying the operator on the state for a small displacement. When the state is displaced by the length of a sub-Planck structure, the two states become quasiorthogonal and distinguishable. Hence, it decides the minimum amount of perturbation and force, which the system can detect.

The overlap between the initial and final states in terms of the Wigner distribution is

$$|\langle\Phi^{'}(r,t)|\Phi^{''}(r,t)\rangle|^2=\frac{2}{\pi\hbar}\int_{-\infty}^{\infty}\int_{-\infty}^{\infty}W^{'}(r,p,t)W^{''}(r,p,t)drdp, \tag{11}$$

where prime denotes the state before perturbation and double primes stand for the same after the application of an external perturbation. One can try to find the displaced state and its Wigner function after carrying out a lengthy calculation. The overlap function is oscillatory and the period of each oscillation will give the length of the structure in some particular direction in phase space. This direction is exploited by utilizing the complex form of the coherent-state parameters. One can, in principle, find the length in a number of phase-space directions to have a better idea of the shape of the structure. The method is cumbersome and not worthy to apply in the context of the present application because we need many of such kind of measurements.

In the following, we will investigate how rotational coupling affects the quantum sensitivity. Specifically, we explore the sensitivity limit due to rotational amendment in the vibrating molecule.

A. Mesoscopic superposition states and their sensitivity

In this section, we make a quantitative analysis of the sensitivity of the sub-Planck dimension with rotational coupling. Here, we denote the dimension of the smallest structure by s, which is proportional to $\sim\hbar^2/A$ ($\sim 1/A$ in atomic units), where A is the classical action of the state in phase space [3,11]. The classical action is defined by the product of the effective support of its state in position and momentum spaces: $A\sim\Delta r\times\Delta p$, where $\Delta r=\sqrt{\langle r^2\rangle-\langle r\rangle^2}$ and $\Delta p=\sqrt{\langle p^2\rangle-\langle p\rangle^2}$. These quantities should be evaluated on the basis of the coherent-state wave packet given by Eq. (7).

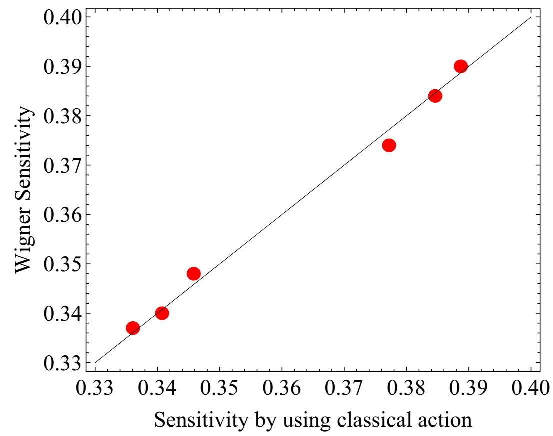

FIG. 3. (Color online) Verification of scaling law between the sensitivity measured from a Wigner plot and numerically calculated by evaluating the classical action. Here, the proportionality factor is 3.78 and slope is 0.99 ($\sim$1.0).

Now it brings out the question of evaluating the sensitivity or the area of the sub-Planck scale structures. In principle, the area can be estimated by either (i) measuring the area of the structures in the phase-space Wigner distribution or (ii) measuring the classical action. The first approach needs a huge computational time to evaluate the Wigner function integral in each case, upon choosing a proper phase-space region. Hence, it should be avoided, when one needs a large number of data. On the other hand, the latter approach requires the proper scaling law between the actual sub-Planck area and the classical action. In our technique, we have made use of both of the approaches to prevail over the situation. In the first step (i), we plot the Wigner function at 1/8th revival time for only six chosen j values (j = 0, 64, 94, 116, 136, 150) and measure the area of sub-Planck structure in each case as a reference value. In step (ii), we compute the inverse of classical actions for the same parameters and, finally, compare with the reference values obtained from Wigner plot. The scaling is depicted in Fig. 3, which produces slope $\sim$1.0. Hence, this is a confirmation of the scaling law: the inverse of the classical action is directly proportional to the quantum sensitivity. Now one would be able to perform a thorough quantitative estimate of the sensitivity. A systematic analysis is performed to quantify the dependence of sensitivity with different rotational angular momentum quantum numbers and at different evolution times.

Variation of sub-Planck dimension with the rotational coupling is shown in Fig. 4. As displayed in Fig. 1, here we keep increasing the value of j up to 160. Figure 4(a) shows the variation of the smallest interference region with rotational amendment for a catlike state. Points depict the

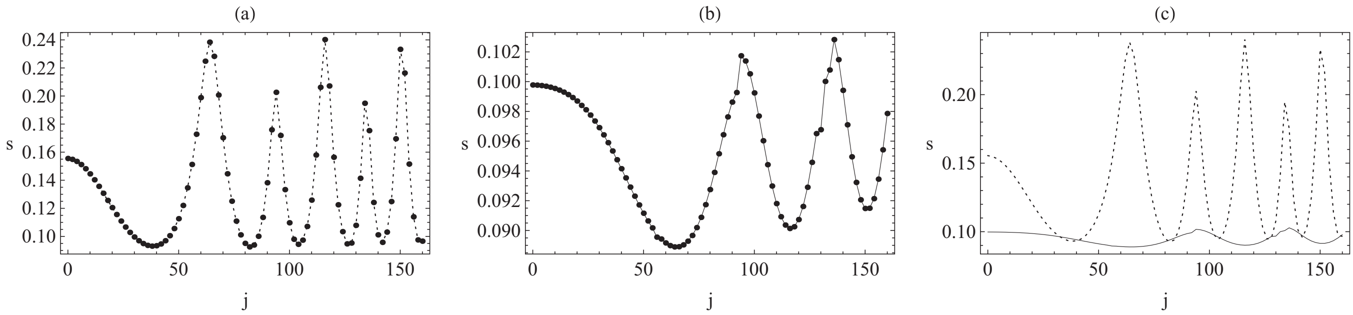

FIG. 4. Variation of the sub-Planck dimension with j: (a) sub-Planck variation in catlike state and (b) sub-Planck variation in compasslike state. (c) Comparison between these two cases.

numerical values of sub-Planck dimensions which vary with the rotational coupling parameter j. It is interesting to see that the variation follows an oscillatory behavior where all the minima represent the high sensitive regions. With increasing value of j, all minima acquire comparatively higher values. In the catlike state, the first minimum occurs at $j = 38$. It is noteworthy to mention that the presence of rotational coupling with particular j values corresponding to the minima shown in Fig. 4 raises the sensitivity limit as compared to the case for $j = 0$. Figure 4(b) gives the variation of the sub-Planck region in a compasslike state. In this case, numerical data show the oscillatory nature where all the minima capture the regions of greater sensitivity. The first minimum corresponds to $j = 64$. A comparison is made between these two cases in Fig. 4(c). It shows that the compasslike state brings out the maximum sensitive state. A detailed study is given in Fig. 5. In the catlike state, minima or the most sensitive sub-Planck dimensions are depicted by the points which are joined by a solid line. It shows that $j = 82$ brings out the most sensitive region in the catlike state. In the compasslike state, minima are joined by a dotted line and it shows that the most sensitive sub-Planck region arises at the first minimum corresponding to $j = 64$. In the next section, further study involves the examination of the orientation of the system in phase space due to rotational coupling.

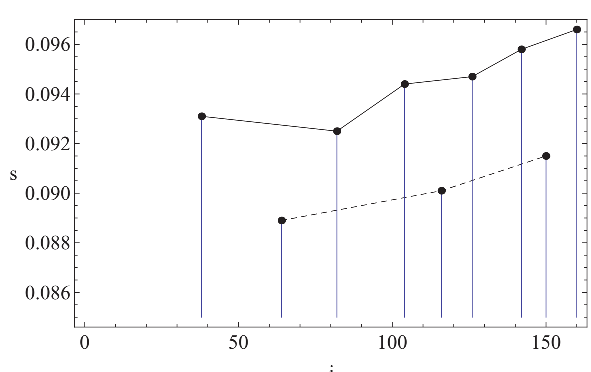

FIG. 5. (Color online) Points show the variation of all minima or most sensitive sub-Planck structures in catlike and compasslike states. The solid line is drawn for catlike-state minima where alternate points depict maximum sensitivity. Among them, second minima corresponding to $j = 82$ gives the most sensitive sub-Planck region in the catlike state. The dotted line shows the compasslike-state minima variation, where it brings out the most sensitivity for $j = 64$, occurs in the first minima.

B. Angle of rotation

The rotational quantum number introduces rotation of the wave packet in phase space, and in the above section we have found the states with maximum sensitivity for some particular values of the rotational quantum number. Hence it is worth finding out the exact amount of rotation ϕ corresponding to the states of maximum sensitivity. Here, we provide a numerical estimation of this rotation angle. It is well known that $\hat{J}_0$ is the generator of rotation and is related to the angular momentum [32]. The corresponding rotation operator would be $U = e^{i\hat{J}_0\phi}$. This operator upon operating on the initial wave packet gives

$$U\Phi(y,t)_{j=0} = \sum_{n=0}^{n'} d_n^0 e^{i(n-\bar{\lambda}_j+1/2)\phi}\psi_{n,0}e^{-iE_{n,0}t} = \chi(y,t). \tag{12}$$

The resulting state is rotated by an angle, depending implicitly on j.

There is a one-to-one correspondence between the above state and the wave packet $\Phi(y,t)$, directly obtained from the time evolution. Hence we find the angle of rotation by maximizing the overlap $|\langle\chi(y,t)|\Phi(y,t)\rangle|^2$ for a given j. Numerically estimated angles of rotation for specific important values of j are shown in Table I. The catlike states reveal maximum sensitivity for $j = 82$ for which the rotation angle is found to be $0.72\,\pi$. The angle for the most sensitive compasslike state ($j = 64$) is 0.22π.

TABLE I. Angle of rotation of the wave packet corresponding to the black dots in Fig. 5 for both catlike and compasslike states.

Catlike state		Compasslike state	
j	ϕ	j	ϕ
38	$0.16\,\pi$	64	$0.22\,\pi$
82	$0.72\,\pi$		
104	$1.16\,\pi$	116	$0.72\,\pi$
126	$1.71\,\pi$		
142	$2.16\,\pi$	150	$1.21\,\pi$
160	$2.77\,\pi$		

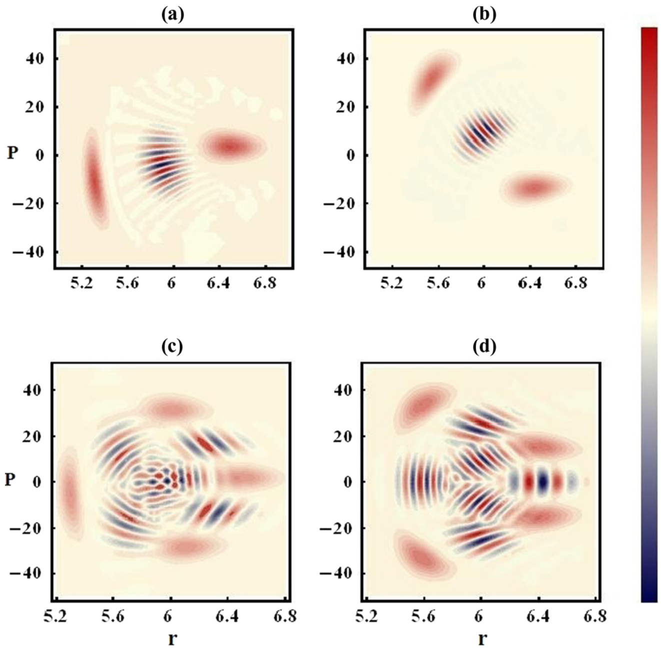

FIG. 6. (Color online) Time evolution of the Wigner function of the CS. The first row shows the catlike state at $t = T_{\rm rev}/4$ for (a) $j = 0$ and (b) $j = 82$, and the second row shows the compasslike state at time $t = T_{\rm rev}/8$ for (c) $j = 0$ and (d) $j = 64$. (d) The mesoscopic superposition of maximum sensitivity in Rotating Morse potential.

C. Phase-space picture

To obtain greater insight into what has been predicted in the previous section, we again invoke the phase-space picture. Figures 6(a) and 6(b) display the Wigner distribution functions of the catlike state for $j = 0$ and $j = 82$, respectively. Figure 6(b) clearly shows rotation of the wave packet in phase space due to rovibrational coupling. It shows 0.72π rotation in the anticlockwise direction. Similarly, Figs. 6(c) and 6(d) show the Wigner distribution functions of the compasslike state for $j = 0$ and $j = 64$, respectively. Following the sensitivity study, we found that the compasslike state for $j = 64$ provides the maximum precision in this rotating Morse system. Although rotation of this particular state is obtained as 0.22π from Table I, there is another crucial factor: the ratio of the revival and classical time scales. This ratio is not an exact integer in most cases and the extra fraction introduces an additional phase in the evolution. The extra rotation is calculated to be 0.029π at $1/8\ T_{\rm rev}$. When added to the rotation due to j, the resulting state is expected to rotate by $0.249\pi \sim 1/4\ \pi$, which is in conformity with the Wigner function in Fig. 6(d).

IV. CONCLUSION

Proper resource accounting is crucial when investigating the precision or sensitivity in quantum systems and formulating the ultimate limits in quantum metrology. In this study, we have considered the rotational coupling in the vibrating diatomic molecule (I_2) and explored the sensitivity of mesoscopic superposition structures. Special attention is paid to catlike and compasslike states where sub-Planck scale structures exist in the quantum interference region. Our sensitivity analysis of quantum interference structures reveals the fact that rotational coupling enhances the sensitivity limit in a vibrating diatomic molecule. We have also identified the rotational levels corresponding to the maximum sensitivity limit. Our study avoids the complication of six-dimensional phase space for rovibrational dynamics of a diatomic molecule. The 1D rotating Morse potential can well capture the rotational effect throughout the time evolution in phase space. Moreover, we provide a quantitative measure of the angle of rotation for different angular momentum states. Our numerical result shows a nice correspondence between the angle of rotation and the phase-space Wigner representation. This study leads to an enhancement in the sensitivity limit and hence provides improvement in the Heisenberg limit for quantum metrology, which is not possible without rotational amendment.

ACKNOWLEDGMENTS

S.G. acknowledges the support provided by DST, Government of India (Fast Track Project No. SR/FTP/PS-062/2010). The authors also acknowledge Professor J. Banerji for giving valuable suggestions.

[1] V. Giovannetti, S. Lloyd, and L. Maccone, Nat. Photon. **5**, 222 (2011); B. M. Escher, R. L. de Matos Filho, and L. Davidovich, Nat. Phys. **7**, 406 (2011).
[2] A. J. Scott and Carlton M. Caves, Ann. Phys. (NY) **323**, 2685 (2008).
[3] W. H. Zurek, Nature (London) **412**, 712 (2001).
[4] G. S. Agarwal and P. K. Pathak, Phys. Rev. A **70**, 053813 (2004).
[5] F. Toscano, D. A. R. Dalvit, L. Davidovich, and W. H. Zurek, Phys. Rev. A **73**, 023803 (2006).
[6] D. A. R. Dalvit, R. L. de M. Filho, and F. Toscano, New J. Phys. **8**, 276 (2006).
[7] S. Ghosh, A. Chiruvelli, J. Banerji, and P. K. Panigrahi, Phys. Rev. A **73**, 013411 (2006).
[8] J. R. Bhatt, P. K. Panigrahi, and M. Vyas, Phys. Rev. A **78**, 034101 (2008).
[9] J. Banerji, Contemp. Phys. **48**, 157 (2007).
[10] S. Ghosh, U. Roy, C. Genes, and D. Vitali, Phys. Rev. A **79**, 052104 (2009).
[11] U. Roy, S. Ghosh, P. K. Panigrahi, and D. Vitali, Phys. Rev. A **80**, 052115 (2009).
[12] S. Ghosh and I. Marzoli, Int. J. Quant. Inf. **9**, 1519 (2011).
[13] S. Ghosh, Int. J. Quant. Inf. **10**, 1250014 (2012).
[14] P. K. Panigrahi, A. Kumar, U. Roy, and S. Ghosh, AIP Conf. Proc. **1384**, 84 (2011).
[15] A. M. Perelomov, *Generalized Coherent States and Their Applications* (Springer, Berlin, 1986).
[16] K. Hosaka, H. Shimada, H. Chiba, H. Katsuki, Y. Teranishi, Y. Ohtsuki, and K. Ohmori, Phys. Rev. Lett. **104**, 180501 (2010).
[17] I. A. Walmsley, Physics **3**, 38 (2010).

[18] H. Katsuki, K. Hosaka, H. Chiba, and K. Ohmori, Phys. Rev. A **76**, 013403 (2007).
[19] K. Ohmori, H. Katsuki, H. Chiba, M. Honda, Y. Hagihara, K. Fujiwara, Y. Sato, and K. Ueda, Phys. Rev. Lett. **96**, 093002 (2006).
[20] J. Banerji and S. Ghosh, J. Phys. B: At. Mol. Opt. Phys. **39**, 1113 (2006).
[21] Y. Cao, L. Zhang, Y. Yang, Z. Sun, and Z. Wang, Chem. Phys. Lett. **442**, 53 (2007).
[22] T. Lohmuller *et al.*, J. Chem. Phys. **120**, 10442 (2004).
[23] C. E. Burkhardt and J. J. Leventhal, Am. J. Phys. **75**, 686 (2007).
[24] M. Duff and H. Rabitz, Chem. Phys. Lett. **53**, 152 (1978).
[25] I. R. Elsum and R. G. Gordon, J. Chem. Phys. **76**, 5452 (1982).
[26] J. Stanek and J. Konaski, Int. J. Quant. Chem. **103**, 10 (2005).
[27] K. Tara, G. S. Agarwal, and S. Chaturvedi, Phys. Rev. A **47**, 5024 (1993).
[28] W. P. Schleich, *Quantum Optics in Phase Space* (Wiley-VCH, Berlin, 2001), and references therein.
[29] M. Tsubouchi, A. Khramov, and T. Momose, Phys. Rev. A **77**, 023405 (2008).
[30] C. Wu, G. Zeng, Y. Gao, N. Xu, L. Y. Peng, H. Jiang, and Q. Gong, J. Chem. Phys. **130**, 231102 (2009).
[31] R. M. Bowman, M. Dantus, and A. H. Zewail, Chem. Phys. Lett. **161**, 297 (1989).
[32] S. H. Dong, R. Lemus, and A. Frank, Int. J. Quantum Chem. **86**, 433 (2002).
[33] I. Sh Averbukh and N. F. Perelman, Phys. Lett. A **139**, 449 (1989).
[34] R. W. Robinett, Phys. Rep. **392**, 1 (2004), and references therein.
[35] H. Katsuki, H. Chiba, B. Girard, C. Meier, and K. Ohmori, Science **311**, 1589 (2006).
[36] H. Katsuki, H. Chiba, C. Meier, B. Girard, and K. Ohmori, Phys. Rev. Lett. **102**, 103602 (2009).
[37] W. Schleich and J. A. Wheeler, Nature (London) **326**, 574 (1987); W. Schleich, D. F. Walls, and J. A. Wheeler, Phys. Rev. A **38**, 1177 (1988).